JASMAC
Conference of the Japan Society of Microgravity Appllication
JSMA

OR 1-5

軌道上燃料ステーションの複数タンクによる燃料スロッシングを考慮した振動抑制制御の検討

Study of vibration suppression control considering fuel sloshing caused by multiple tanks of an on-orbit fuel station

小林大輝 [1]，中西洋喜 [2]
DAIKI KOBAYASHI[1], HIROKI NAKANISHI[1]
[1] 東京科学大学， Institute of Science Tokyo
* kobayashi.d.06d6@m.isct.ac.jp

Abstract: One of the main resons for the limitaion of a spacecraft's end of life is the depletion of fuel. Therefore, orbit refueling, targeting launch vehicles or satellites, has been attracting attention. In recently, various companies challenge to develop and demonstrate orbital refueling. There are some concept that fuel station equipped with mulplt tank. However, fuel sloshing caused by multiple fuel tanks is little concerned, despite it can adversely affect docking attitude and position. In this study, we applied the Multi Pulsating Ball Model (MPBM) to multiple tanks and simulated attitude control during orbit refuel docking. We applied quaternion feedback control, LQR control, and iterative-LQR control, and their performances were evaluated from viewpoint of common refueling interface docking feasibility .

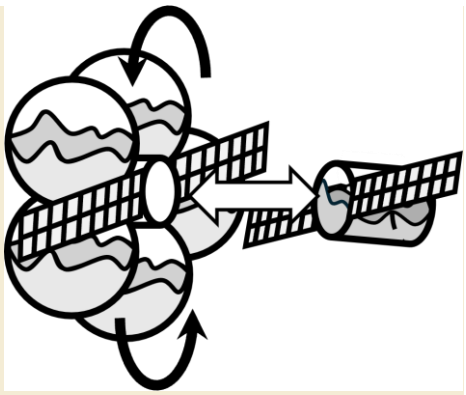

Keywords: orbit servicing, orbit refueling, fuel sloshing, Multiple Pulsating Ball Model, attitude control, LQR, iterative-LQR

1. Introduction

One of the main reasons for the limitation of a spacecraft's end of life is the depletion of fuel. This restricts the operation of satellite constellations, deep space exploration missions, and other missions. For instance, despite remaining functional, the Intelsat-901 satellite was decommissioned due to fuel exhaustion. To address this issue, technologies for extending satellite life, such as orbital refueling, were proposed and demonstrated. For example, the world's first automated satellite-to-satellite orbit refueling was demonstrated in Orbital-Express mission[1)] by DARPA in 2007. In recent years, satellite development and reusable rocket technologies have matured significantly in commercial companies such as SpaceX. In this context, orbit refueling technologies have been attracting considerable attention for sustainable satellite development[2)]. For example, Orbit Fab developed Tanker-01, equipped with a common refueling interface[3)], which was launched in 2021. Such orbital refueling systems are expected to be promising technologies for extending the operational lifetime of spacecraft.

In the future, efficient Mars exploration is expected to be enabled in situ resources utilization (ISRU) technologies, such as extracting and using water from the Moon[4)]. The Moon's gravity is 1/6 that of Earth's, making it efficient to use hydrogen and oxygen mined on the Moon to refuel Mars exploration

vehicles. It has been proposed that orbit refueling stations be positioned at the Earth-Moon Lagrange point 1, as this location minimizes fuel loss[5].

Orbital refueling is generally proposed to consist of a sequence of operations: rendezvous, docking, fuel transfer, orbital separation[3]. From the viewpoint of safety and leakage prevention, satellites to be refueled are required to align precisely with the docking interface. This imposes strict requirements on the attitude and position control of the refueling spacecraft. However, compared with conventional spacecraft, orbit refueling stations are equipped with multiple large fuel tanks, raising concerns about disturbances to attitude and position control caused by fuel sloshing.

As conventional countermeasures against fuel sloshing, bladders, diaphragms, and propellant management devices (PMDs) have been proposed and applied[7]. However, there are challenges, such as difficulties in developing large elastomer membranes and degradation due to repeated refueling. In addition, cryogen fuel such as liquid hydrogen and liquid oxygen have low surface tension, making it difficult for PMDs to effectively suppress fuel sloshing.

Under these circumstances, we considered suppressing fuel sloshing through spacecraft attitude control. There have been many studies on sloshing suppression via attitude control using various mechanical models. However, few studies have addressed orbital refueling stations equipped with multiple large tanks. In this study, we modeled the dynamics of an orbital refueling station with multiple large tanks and applied several control methods, including quaternion feedback control, linear quadratic regulator (LQR) control, and iterative LQR control. Finally, we compare the performance of these control methods from the viewpoint of docking suitability with the existing common docking interface.

2. Sloshing and Satellite dynamics

In this section, we present the fuel sloshing model and the satellite dynamics model under microgravity conditions. Vreeburg proposed the Multi Pulsating Ball Model (MPBM) [8] and demonstrated it in orbit[9]. In this model, the sloshing mass is represented as a three-dimensional pendulum whose radius changes over time. The sloshing mass is modeled as a spherical fuel slug, which experiences friction and a nominal force from the tank wall. The variation in the slug's radius represents the expansion and contraction caused by surface tension.

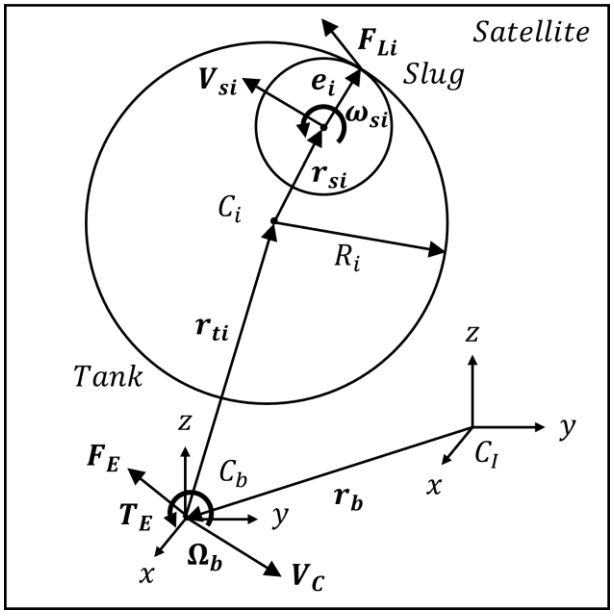

Figure 1 . Schematic diagram of MPBM about ith tank

We present the variables for the ith tank and the satellite. We define C_I as the center of mass of the satellite system. C_b denotes the center of mass of the satellite body, C_i denotes the center of the ith tank. r_b is the vector from the system center of mass to the satellite body's center of mass, and r_{ti} is the vector from the satellite's center of mass to the ith tank's center. The satellite velocity is denoted by V_C, and the velocity of the ith slug is denoted by V_{si}. The angular velocity of the satellite body is Ω, and the angular

velocity of the $\boldsymbol{i}$th slug is $\boldsymbol{\omega_{si}}$. $\boldsymbol{F_{Li}}$ represents the force from tank wall, and $\boldsymbol{T_{Li}}$ represents the torque from the tank wall. Finally, $\boldsymbol{e_i}$ is the unit vector from the $\boldsymbol{i}$th tank center toward the slug, and $\boldsymbol{R_i}$ is the radius of the $\boldsymbol{i}$th tank.

2.1. The equation of motion of a satellite

We derive the equations of motion for the satellite system by considering both the sloshing mass and the satellite body dynamics. Vreeburg proposed MPBM[8] for a single tank, and Deng extended the model to multiple tanks[10]. Based on these studies, we derive the equation of motion using the satellite system coordinates as the inertial frame. The notation $(\cdot)$ denotes differentiation with respect to the satellite body frame, while (d/dt) denotes differentiation with respect to the inertial frame. Equations (1) and (2) present the rotational and translational equations of motion for the satellite body. Equations (3) and (4) present the rotational and translational equations of motion for the $\boldsymbol{ith}$ sloshing mass.

$$M\frac{d\boldsymbol{V_c}}{dt} = \sum_{n=1}^{i}\boldsymbol{F_{Li}} + \boldsymbol{F_E} \tag{1}$$

$$\boldsymbol{I_b}\cdot\dot{\boldsymbol{\Omega}} + \boldsymbol{\Omega}\times(\boldsymbol{I_b}\cdot\boldsymbol{\Omega}) = \boldsymbol{r_E}\times\boldsymbol{F_E} + \boldsymbol{T_E} + \sum_{n=1}^{i}\boldsymbol{T_{Li}} + \sum_{n=1}^{i}[(R_i\boldsymbol{e_i} + \boldsymbol{r_{ti}})\times\boldsymbol{F_{Li}}] \tag{2}$$

$$m_{si}\left[\frac{d\boldsymbol{V_c}}{dt} + \dot{\boldsymbol{V}}_{\boldsymbol{s\imath}} + \dot{\boldsymbol{\Omega}}\times(\boldsymbol{r_{si}} + \boldsymbol{r_{ti}}) + \boldsymbol{\Omega}\times(\boldsymbol{\Omega}\times\boldsymbol{r_{si}}) + 2\boldsymbol{\Omega}\times\boldsymbol{V_{si}} + \boldsymbol{\Omega}\times(\boldsymbol{\Omega}\times\boldsymbol{r_{ti}})\right] = -\boldsymbol{F_{Li}} \tag{3}$$

$$\frac{2}{5}m_{si}(R_i - r_i)\left[(-2\dot{r}_i)(\boldsymbol{\omega_{si}} + \boldsymbol{\Omega}) + (R_i - r_i)\left(\dot{\boldsymbol{\omega}}_{\boldsymbol{s\imath}} + \dot{\boldsymbol{\Omega}} + \boldsymbol{\Omega}\times\boldsymbol{\omega_{si}}\right)\right] = -\boldsymbol{T_{Li}} - (R_i - r_i)\boldsymbol{e_i}\times\boldsymbol{F_{Li}} \tag{4}$$

$$\boldsymbol{w} = \boldsymbol{e}\times\dot{\boldsymbol{e}}_{\boldsymbol{\imath}} = \boldsymbol{e}\times\frac{\dot{\boldsymbol{r}}_{\boldsymbol{s\imath}}}{\boldsymbol{r_i}} = \boldsymbol{e_i}\times\frac{\boldsymbol{V_{si}}}{\boldsymbol{r_i}} \tag{5}$$

From Equation (5), the satellite body acceleration, as well as the velocity and acceleration of each tank's sloshing mass, are derived as Equation (6),(7) and (8).

$$\frac{\boldsymbol{dV_c}}{\boldsymbol{dt}} = \ddot{\boldsymbol{r}}_{\boldsymbol{B}} + 2\boldsymbol{\Omega}\times\dot{\boldsymbol{r}}_{\boldsymbol{B}} + \dot{\boldsymbol{\Omega}}\times\boldsymbol{r_B} + \boldsymbol{\Omega}\times(\boldsymbol{\Omega}\times\boldsymbol{r_B}) \tag{6}$$

$$\boldsymbol{V_{si}} = \dot{\boldsymbol{r}}_{\boldsymbol{s\imath}} = \dot{\boldsymbol{r}}_{\boldsymbol{\imath}}\boldsymbol{e_i} + \boldsymbol{r_i}\dot{\boldsymbol{e}}_{\boldsymbol{\imath}} = \dot{\boldsymbol{r}}_{\boldsymbol{\imath}}\boldsymbol{e_i} + \boldsymbol{r_i}\boldsymbol{w_i}\times\boldsymbol{e_i} \tag{7}$$

$$\dot{\boldsymbol{V}}_{\boldsymbol{s\imath}} = \ddot{\boldsymbol{r}}_{\boldsymbol{s\imath}} = \ddot{\boldsymbol{r}}_{\boldsymbol{\imath}}\boldsymbol{e_i} + 2\boldsymbol{r_i}\boldsymbol{w_i}\times\boldsymbol{e_i} + \boldsymbol{r_i}\boldsymbol{w_i}\times(\boldsymbol{w_i}\times\boldsymbol{e_i}) \tag{8}$$

The counterforce from tank wall, $\boldsymbol{F_{Li}}$ is expressed in terms of tank's nominal force $\boldsymbol{N_i}$, the tank radius unit vector $\boldsymbol{e_i}$, and the friction force $\boldsymbol{F_{bi}}$ from the wall.

$$\boldsymbol{F_{Li}} = \boldsymbol{N_i}\boldsymbol{e_i} + \boldsymbol{F_{bi}} \tag{9}$$

Inner product Equation (9) and $\boldsymbol{e_i}$ is expressed as.

$$\mathbf{m_{si}}\left[\frac{\mathbf{dV_c}}{\mathbf{dt}} + \dot{\boldsymbol{V}}_{\boldsymbol{s\imath}} + \dot{\boldsymbol{\Omega}}\times(\boldsymbol{r_{si}} + \boldsymbol{r_{ti}}) + \boldsymbol{\Omega}\times(\boldsymbol{\Omega}\times\boldsymbol{r_{si}}) + 2\boldsymbol{\Omega}\times\boldsymbol{V_{si}} + \boldsymbol{\Omega}\times(\boldsymbol{\Omega}\times\boldsymbol{r_{ti}})\right]\cdot\boldsymbol{e_i} = -\boldsymbol{F_{Li}}\cdot\boldsymbol{e_i} = -\boldsymbol{N_i} \tag{10}$$

The nominal force $\boldsymbol{N_i}$ acts along the slosh radius. The expansion and contraction energy is denoted[11] as $\boldsymbol{T_b}$, the rotational energy as $\boldsymbol{T_a}$, surface tension energy as $\boldsymbol{T_s}$. Defining the slug radius vector magnitude as $\boldsymbol{R_{si}} = (\boldsymbol{R_i} - \boldsymbol{r_i})$

$$\boldsymbol{T_b} = \frac{\mathbf{3}}{\mathbf{10}}\boldsymbol{m_{si}}\dot{\boldsymbol{R}}_{\boldsymbol{s\imath}}^{\,2}, \boldsymbol{T_a} = \frac{\mathbf{1}}{\mathbf{5}}\boldsymbol{m_{si}}\boldsymbol{R_{si}^2}(\boldsymbol{\omega_{si}} + \boldsymbol{\Omega})^2, \boldsymbol{T_s} = 4\boldsymbol{\pi\sigma}\boldsymbol{R_{si}^2}$$

From the viewpoint of work, the forces acting on the sloshing mass perform mechanical work that can be related to its kinetic and potential energy through the work-energy principle.

$$\boldsymbol{N_i}(-\boldsymbol{dR_{si}}) = \boldsymbol{dT_b} - \boldsymbol{dT_a} - \boldsymbol{dT_s}$$

$$= \frac{3}{5} m_{si} \ddot{R}_{si} dR_{si} - \frac{2}{5} m_{si} R_{si} (\omega_{si} + \Omega)^2 dR_{si} - 8\pi\sigma R_{si} dR_{si}$$

$$N_i = \frac{3}{5} m_{si} \ddot{r}_i + \frac{2}{5} m_{si} (\omega_{si} + \Omega)^2 (R_i - r_i) + 8\pi\sigma (R_i - r_i) \quad (11)$$

Substituting $\ddot{r}_i$ from Equation (11) into (8), and rearranging Equation (10), the nominal force N_i is obtained as Equation (12).

$$N_i = -\frac{3}{8} m_{si} \frac{dV_c}{dt} e_i + \frac{3}{8} m_{si} r_i [e_i \times (\Omega + w)]^2 + \frac{1}{4} m_{si} (R_i - r_i)(\Omega + \omega_{si})^2 - 5\pi\sigma (R_i - r_i) \quad (12)$$

then, friction force F_{bi}[9)]

$$F_{bi} = \frac{f_b \mu m_{si}}{r_{si}^2} V_u$$

$$= - \frac{f_b \mu m_{si}}{r_{si}^2} e_i \times (e_i \times V_{si} + R_i \omega_{si})$$

The coefficient f_b is determined experimentally, in this study, $f_b = 0.2$.

The sloshing slug radius has a minimum limit, ($L_{min} = R_i - r_{max}$), beyond which the slug is considered frozen[8)]. In this situation, the change in the sloshing mass radius stops, i.e.,$\dot{r}_i = \ddot{r}_i = 0$, and the nominal force is given by Equation (10). For the initial condition, the sloshing mass is stabilized and thus frozen. Therefore, we use Equation (10) for the nominal force.

Finally, by simplifying these equations, we obtain the equation of motion for the multiple-tank fuel station.

$$x = [r_B, \dot{r}_B, \Omega, V_{s0}, \dots, V_{sn}, \omega_{s0}, \dots \omega_{sn}, e_0, \dots, e_n, r_0, \dots, r_n, q_B, q_{s0}, \dots, q_{sn}]^T$$

$$C(x)\dot{x} = A(x) + Bu$$

$$\dot{x} = C(x)^{-1} A(x) + C^{-1}(x) Bu \quad (12)$$

We calculate C^{-1} using the python CasADi library. $A(x), B, u$ **and** $C(x)$ are given in the Appendix. By substituting $f(x) = C(x)^{-1} A(x)$, **and** $g(x) = C(x)^{-1} B$, we obtain the nonlinear equation of motion.

$$\dot{x} = f(x) + g(x)u$$

We simulated the satellite attitude control by integrating these equations using fourth-order Runge-Kutta algorithm. In this study, $\dot{r}_i = \ddot{r}_i = 0$ for simplification, meaning that the sloshing mass radius is constant. The control torque T_E, and control force F_E are generated by external torques and forces.

3. The control simulation of a multiple-tank refueling satellite

The simulation parameters are listed in Table 1. The tank fill ratio is set to 40 %, and the sloshing mass ratio to 20 %[8)]. Various liquid fuels are considered, including water, hydrogen, oxygen, and hydrazine. The physical parameters are shown in Table 1.

Table 1. satellite parameter

parameter	variable	value	parameter	variable	value
Tank num	n	4	Satellite inertia	I_B	$\mathbf{diag}(500, 500, 500)$
radius	R_i	1.0 m	Initial fuel position	e_i	[0, 0, -1]
Cener of tank	r_{ti}	[0, 0, ±1.5] m [0, ±1.5, 0] m	Sloshing mass	m_{si}	H2O : 334 kg N2H4 : 339 kg

Satellite mass	$\boldsymbol{M}$	1000 kg			LH2 : 23.7 kg LO2 : 382 kg

Table 2. fuel parameter

	density [kg/m^3]	Surface tension [N/m]	viscosity [Pa·s]
water（H2O）	997	$\mathbf{72.0 \times 10^{-3}}$	$\mathbf{1.0 \times 10^{-3}}$
hydrazine（N2H4）	1013	$\mathbf{65.1 \times 10^{-3}}$	$\mathbf{8.76 \times 10^{-4}}$
Liquid hydrogen（LH2）	70.8	$\mathbf{2.0 \times 10^{-3}}$	$\mathbf{1.58 \times 10^{-4}}$
Liquid oxygen（LO2）	1141	$\mathbf{13.2 \times 10^{-3}}$	$\mathbf{5.85 \times 10^{-5}}$

Fig.2 shows the schematic diagram of a refueling station. The target attitude is set to a rotation about the x-axis, as fuel sloshing is assumed to be most severe along this axis. Two rotation angles were considered: 10 degrees and 45 degrees. The 10 degrees case represents the attitude error between the fuel station and the fuel receiver, while the 45 degrees case represents the worst-case scenario for attitude control. The corresponding target quaternion are $\boldsymbol{q_t} \simeq [\mathbf{0.087, 0, 0, 0.996}]^{\boldsymbol{T}}$ **and** $[\mathbf{0.383, 0, 0, 0.924}]^{\boldsymbol{T}}$, respectively. The target satellite angular velocity is $\boldsymbol{\Omega_t} = [\mathbf{0, 0, 0}]^{\boldsymbol{T}}$.

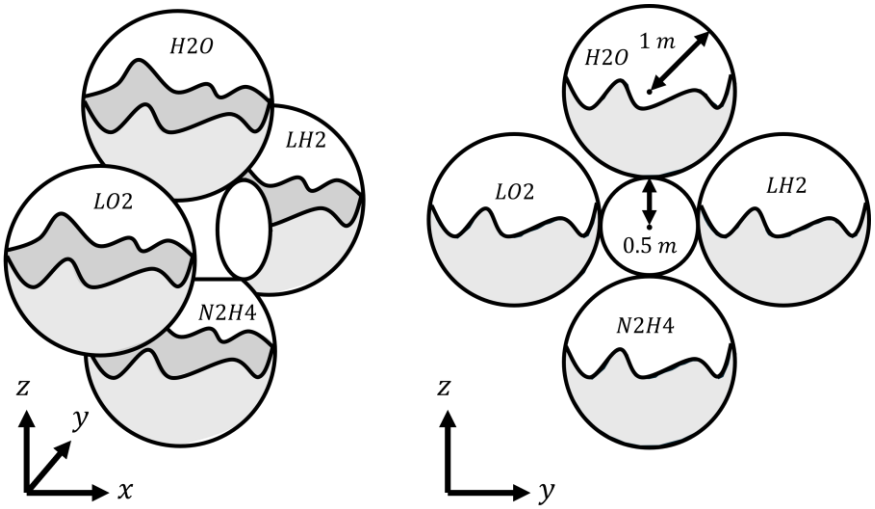

Figure 2. Schematic diagram of a refuel station

3.1. Attitude control by quaternion feedback

First, we conducted attitude control without considering satellite's internal fuel sloshing. The quaternion feedback determined the control input $\boldsymbol{u}$ as follows:

$$\boldsymbol{u} = -K_p \boldsymbol{q_B} \otimes \boldsymbol{q_t^{-1}} - K_d(\boldsymbol{\Omega} - \boldsymbol{\Omega_t})$$

Fig.3,4 shows $K_p = 10, K_d = 100$ results

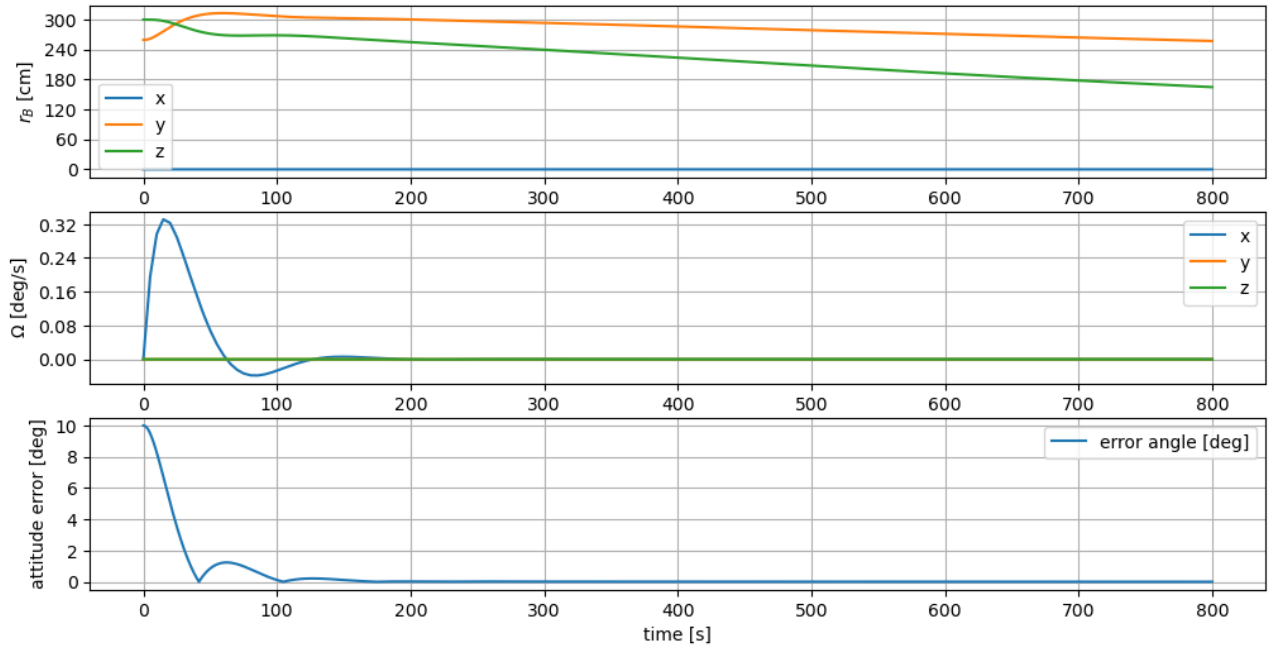

Figure 3. 10 degrees rotation around the x-axis by quaternion feedback

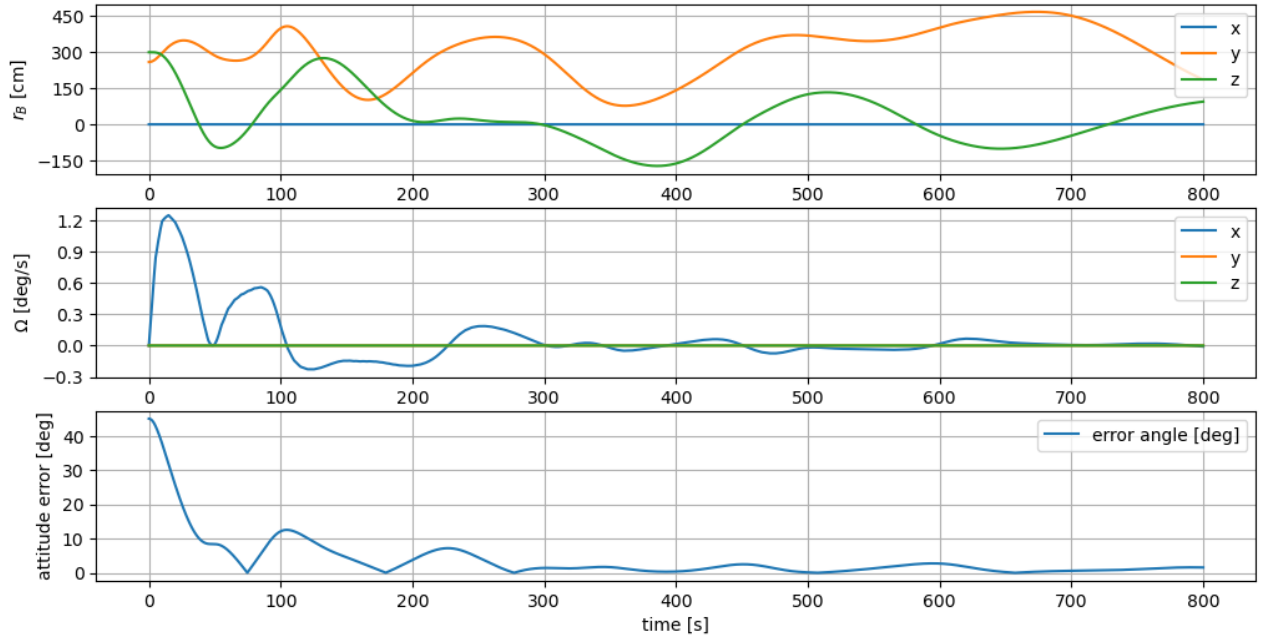

Figure 4. 45 degrees rotation around the x-axis by quaternion feedback

From these results, the refueling station achieved 10 degrees of rotation around the x-axis using quaternion feedback control within 200 seconds. However, after attitude control, the satellite body exhibited a translational motion of approximately 1 mm/s caused by fuel sloshing. For the 45-degree rotation case, the station could not achieve the desired attitude within 800 seconds. In addition, the satellite body oscillated at approximately ± 10 cm/s in velocity and ± 50 cm in position. These results are attributed to the fact that quaternion feedback control does not account for translational motion caused by fuel sloshing. The existing common refueling interface[12] allows a misalignment of ± 10 mm. Therefore, these results indicated that the refueling station could not successfully dock using quaternion feedback control alone.

3.2. Rotation and Transaction control by LQR control

Next, we conducted satellite rotational and transactional control using the LQR method. LQR control is an optimal control approach for linear control systems like Equation (13). The optimal input gain is obtained by solving the Riccati equation, as given in Equation (14).

$$\dot{\boldsymbol{x}} = \boldsymbol{Ax} + \boldsymbol{Bu} \tag{13}$$

$$\boldsymbol{PA} + \boldsymbol{A}^T\boldsymbol{P} - \boldsymbol{PBR}^{-1}\boldsymbol{B}^T\boldsymbol{P} + \boldsymbol{Q} = \boldsymbol{0} \tag{14}$$

$$\boldsymbol{u} = -\boldsymbol{R}^{-1}\boldsymbol{B}^T\boldsymbol{Px} \tag{15}$$

Equation (12) includes extra state variables. Therefore, we selected the control variables as $\boldsymbol{x}' = [\boldsymbol{r_B}, \dot{\boldsymbol{r}}_{\boldsymbol{B}}, \boldsymbol{\Omega}, \boldsymbol{q_B}]^T$. These variables represent the satellite body's rotational and translational motion. Equation (16) expresses the modified satellite equation of motion. Since this equation is also nonlinear, we linearized it around the initial conditions $\boldsymbol{x_0}$.

$$\dot{\boldsymbol{x}}' = \boldsymbol{f}(\boldsymbol{x}') + \boldsymbol{g}(\boldsymbol{x}')\boldsymbol{u}' \tag{16}$$

$$\dot{\boldsymbol{x}}' = \frac{\partial \boldsymbol{f}(\boldsymbol{x}')}{\partial \boldsymbol{x}'}|_{\boldsymbol{x_0}}\boldsymbol{x}' + \boldsymbol{g}(\boldsymbol{x_0})\boldsymbol{u}'$$

We define $\boldsymbol{A} = \frac{\partial \boldsymbol{f}(\boldsymbol{x}')}{\partial \boldsymbol{x}'}|_{\boldsymbol{x_0}}\boldsymbol{B} = \boldsymbol{g}(\boldsymbol{x_0})$, and substitute Equation (14) and (15), and obtain input $\boldsymbol{u}$

Fig.5 and Fig.6 show the result for $\boldsymbol{R} = diag(10,10,10), \boldsymbol{Q} = diag(100,100,100)$.

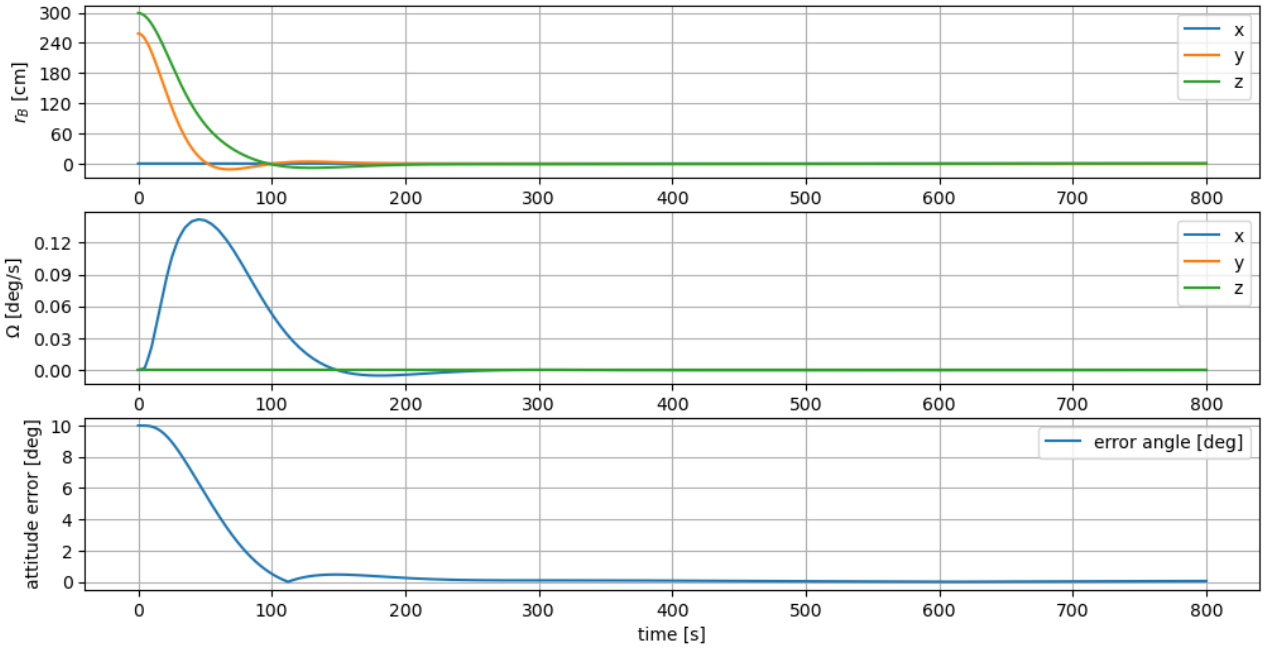

Figure 5. 10 degrees rotation around the x-axis by LQR control

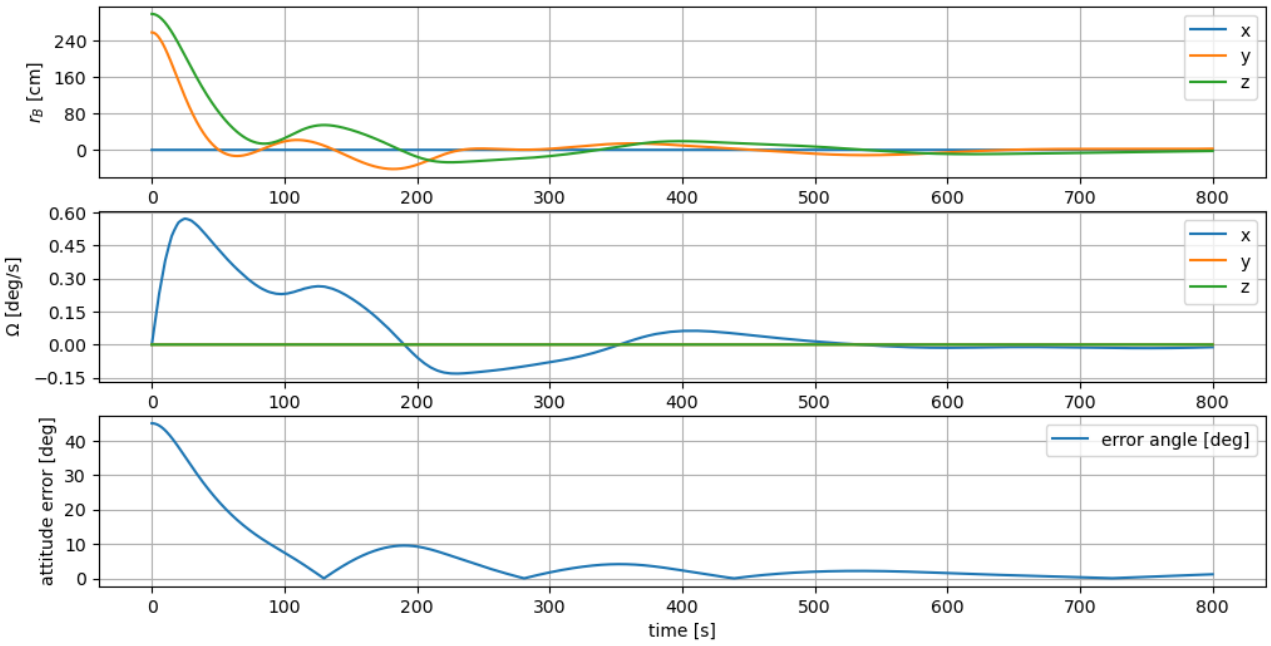

Figure 6. 45 degree rotation around the x-axis by LQR control

From Fig.5 and Fig.6, it is observed that LQR control can suppress satellite translational motion caused by fuel sloshing. Fig.5 shows that the translational motion was suppressed within ± 10 mm, indicating that docking with the existing common refuel interface would be feasible. However, Fig.6 shows that the translational motion could not be suppressed within ± 10 mm, and that oscillations remained after 800 seconds. This is considered that LQR control uses linearized state equations, making it unsuitable for large-angle attitude maneuvers.

3.3. Rotation and Transaction control by iterative-LQR control

Since it is difficult to perform translational control using linearized state equation, we applied iterative LQR control (iLQR). Thid method is a type of Differential Dynamic Programming (DDR) and is used for solving unconstrained nonlinear optimal control problems[31, 14]. This method computes the control input that satisfies these optimal problem.

$$\min_U J(x_0, U) = \sum_{i=0}^{N-1} l(x_i, u_i) + l_f^N(x_N)$$
$$subject\ to\ x_{i+1} = f(x_i, u_i), i = 0,1, \dots, N-1$$

$x_i \in R^n\ and\ u_i \in R^m$ denote the state vector and input vector at step i, respectively, N is the prediction horizon. The running cost $l(x_i, u_i)$ and the final cost $l_f^N(x_N)$ are defined as follows

$$l(x_i, u_i) = \frac{1}{2} x_i^T Q x_i + \frac{1}{2} u_i^T R u_i$$
$$l_f^N(x_N) = \frac{1}{2} x_N^T Q_f x_N$$

This optimal control problem is expressed using $X = \{x_0, x_1, \dots, x_N\}, U = \{u_0, u_1, \dots, u_{N-1}\}$ as Equation (16).

$$U^* = arg\min_U J(x_0, U) \tag{16}$$

define $Q_k(x_k, u_k)$ as in Equation (17). This represents the minimum value of the cost function after applying the kth input $\boldsymbol{u_k}$.

$$Q_k(x_k, u_k) = \min_{u_{k+1},\dots,u_{N-1}} \left[\sum_{i=k}^{N-1} l(x_i, u_i) + l_f^N(x_N) \right] \tag{17}$$

define $V_k(x_k, u_k)$ as Equation (18) and (19), where $V_k(x_k, u_k)$ represents the optimal cost from step k to the final step.

$$V_k(x_k) = \min_{u_k} Q_k(x_k, u_k) \tag{18}$$

$$Q_k(x_k, u_k) = l_k(x_k, u_k) + V_{k+1}\big(f(x_k, u_k)\big) \tag{19}$$

$V_i(x_i)$ satisfies the boundary condition $V_N(x_N) = l_f(x_N)$. Therefore, Equation (19) is solved sequentially for $i = N-1, \dots, 0$. To minimize $J(x_0, U)$, minimize $Q_k(x_k, u_k)$ at each step, to minimize $Q_k(x_k, u_k)$, minimize $Q_k(\delta x_k, \delta u_k)$. Thus, obtain second order Taylor expansion of $Q_k(x_k, u_k)$.

$$\begin{aligned} &Q_k(\delta x_k, \delta u_k) \\ &= l_k(x_k + \delta x_k, u_k + \delta u_k) - l_k(x_k, u_k) + V_{k+1}\big(f(x_k + \delta x_k, u_k + \delta u_k)\big) - V_k\big(f(x_k, u_k)\big) \\ &\simeq \frac{1}{2} \begin{bmatrix} 1 \\ \delta x_k \\ \delta u_k \end{bmatrix}^T \begin{bmatrix} 0 & (Q_x^k)^T & (Q_u^k)^T \\ Q_x^k & Q_{xx}^k & Q_{xu}^k \\ Q_u^k & Q_{ux}^k & Q_{uu}^k \end{bmatrix} \begin{bmatrix} 1 \\ \delta x_k \\ \delta u_k \end{bmatrix} \end{aligned}$$

$$Q_x^k = l_x^k + (f_x^k)^T V_x^{k+1}$$

$$Q_u^k = l_u^k + (f_u^k)^T V_x^{k+1}$$

$$Q_{xx}^k = l_{xx}^k + (f_x^k)^T V_{xx}^{k+1} f_x^k + V_x^{k+1} f_{xx}^k$$

$$Q_{ux}^k = l_{ux}^k + (f_u^k)^T V_{xx}^{k+1} f_x^k + V_x^{k+1} f_{ux}^k$$

$$Q_{uu}^k = l_{uu}^k + (f_u^k)^T V_{xx}^{k+1} f_u^k + V_x^{k+1} f_{uu}^k$$

To minimize $Q_k(x_k, u_k)$, minimize $Q_k(\delta x_k, \delta u_k)$

$$\begin{aligned} \delta u^* &= arg \min_{\delta u_i} Q^k(\delta x_k, \delta u_k) \\ &= -(Q_{uu}^k)^{-1}(Q_u^k + Q_{ux}^k \delta x_k) = k_k + K_k \delta x_k \end{aligned}$$

This leads to each variable function V_x, V_{xx} becomes

$$\begin{aligned} V_x^{k+1} &= Q_x^k - K_k^T Q_{uu}^k k_k \\ V_{xx}^{k+1} &= Q_{xx}^k - K_k^T Q_{uu}^k K_k \end{aligned}$$

We obtain the optimal input $\boldsymbol{u_k} + \delta \boldsymbol{u_k^*}$, but this input serves as the initial estimation. Therefore, we repeat same process using a line search ($\alpha < 1$) based on Equation (20) until the cost is minimized.

$$\widehat{u_k} = u_k + \alpha k_k + K_k(\widehat{x_k} - x_k) \tag{20}$$

Fig.7 shows the results of the iLQR control. The final cost weight was set to $Q_f = diag(7.5e4, 7.5e4, 7.5e4)$, the running cost weight to $Q = diag(5e4, 5e4, 5e4)$, and the input cost weight to $R = diag(30, 30, 30)$. The prediction horizon was set to 30 seconds, and the time step to 0.5 seconds. The initial estimated input was chosen as the previous input. Due to computational complexity, the control period was set to 0.2 Hz.

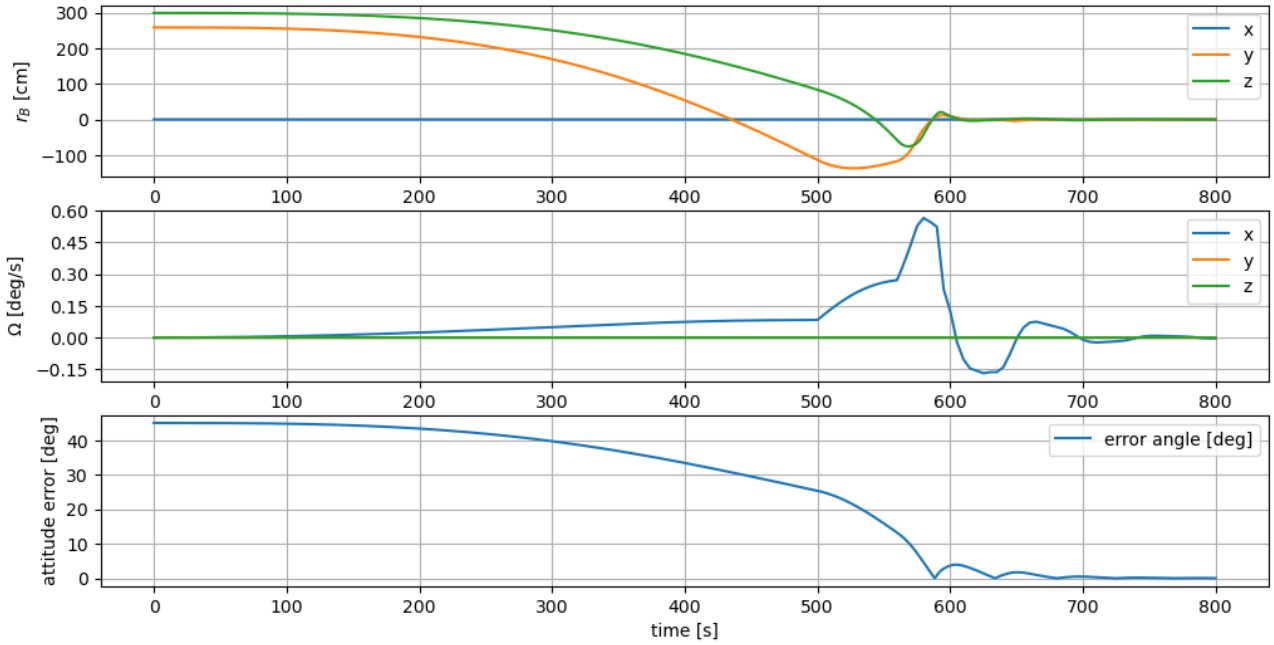

Figure 7. 45 degrees rotation around x axis by iLQR control

From Fig.7, it can be seen that the satellite's translational motion was suppressed to within ±10 mm. This indicated that, after a large-angle attitude maneuver, the refueling station stop with sufficient precision for docking using the existing refueling interface.

4. Conclusion

In this study, we modeled a multiple-tank refueling station using the Multi Pulsating Ball Model (MPBM). Attitude control about a single axis was conducted using this model with quaternion feedback control, LQR control, and iterative-LQR (iLQR) control. Two maneuver cases were examined: a small-angle maneuver of 10 degrees and a large-angle maneuver of 45 degrees. The results showed that, with quaternion feedback alone, translational velocity induced by fuel sloshing affected docking feasibility. Next, LQR control was applied by linearizing the equations of motion, enabling both rotational and translational control. However, LQR control could not sufficiently suppress translational motion to allow docking, likely due to linearization errors. Finally, the nonlinear optimal control method, iterative-LQR. was applied, achieving both rotational and translational control with sufficient precision for docking using the existing common refuel interface.

From these results, it is concluded that LQR control is adequate for small-angle attitude maneuvers. However, for large-angle attitude maneuvers, nonlinear optimal control methods such as iLQR are required to suppress translational motion sufficiently for docking with the existing common refueling interface.

5. Appendix

$$\boldsymbol{A_i} = -\boldsymbol{m_{si}} \boldsymbol{e_i} \boldsymbol{e_i^T}$$

$$\boldsymbol{B_i} = \boldsymbol{m_{si}} \boldsymbol{e_i} \boldsymbol{e_i^T} [\boldsymbol{r_B} + \boldsymbol{r_{ti}}]^{\times}$$

$$\boldsymbol{C_i} = -\boldsymbol{m_{si}} \boldsymbol{e_i} \boldsymbol{e_i^T} [2\boldsymbol{\Omega} \times \dot{\boldsymbol{r}}_{\boldsymbol{B}} + \boldsymbol{\Omega} \times (\boldsymbol{\Omega} \times \boldsymbol{r_B}) + \boldsymbol{\Omega} \times (\boldsymbol{\Omega} \times \boldsymbol{r_{ti}})] + \boldsymbol{m_{si}} \boldsymbol{r_i} [\boldsymbol{e_i} \times (\boldsymbol{\Omega} + \boldsymbol{w_i})] \boldsymbol{e_i} - \frac{\boldsymbol{f_b} \boldsymbol{\mu} \boldsymbol{m_{si}}}{\boldsymbol{r_{si}^2}} \boldsymbol{e_i} \times (\boldsymbol{e_i} \times \boldsymbol{V_{si}} + \boldsymbol{R_i} \boldsymbol{\omega_{si}})$$

$$\boldsymbol{D_i} = \boldsymbol{m_{si}} \boldsymbol{I_{3\times 3}}$$

$$\boldsymbol{E_i} = -\boldsymbol{m_{si}} [\boldsymbol{r_B} + \boldsymbol{r_{ti}} + \boldsymbol{r_i} \boldsymbol{e_i}]^{\times}$$

$$\boldsymbol{F_i} = \boldsymbol{m_{si}} \boldsymbol{I_{3\times 3}}$$

$$\boldsymbol{G_i} = \boldsymbol{m_{si}} \left[2\boldsymbol{\Omega} \times (\dot{\boldsymbol{r}}_{\boldsymbol{B}} + \boldsymbol{V_{si}}) + \boldsymbol{\Omega} \times \left(\boldsymbol{\Omega} \times (\boldsymbol{r_B} + \boldsymbol{r_{ti}} + \boldsymbol{r_i} \boldsymbol{e_i}) \right) \right]$$

$$H_i = (R_i - r_i)[e_i]^{\times} A_i$$

$$I_i = \frac{2}{5} m_{si}(R_i - r_i)^2 + (R_i - r_i)[e_i]^{\times} B_i$$

$$J_i = \frac{2}{5} m_{si}(R_i - r_i)^2$$

$$K_i = \frac{2}{5} m_{si}(R_i - r_i)[-2(V_{si} - r_i w \times e_i)e_i(\Omega + \omega_{si}) + (R_i - r_i)(\Omega \times \omega_{si})] + T_{Li} + (R_i - r_i)[e_i]^{\times} \mathrm{C_i}$$

$$\mathbf{L} = \sum_{i=1}^{N} [\mathrm{r}_{ti} + R_i e_i]^{\times} A_i$$

$$M = \sum_{i=1}^{N} [\mathrm{r}_{ti} + R_i e_i]^{\times} B_i - I_B$$

$$N = \sum_{i=1}^{N} (C_i + T_{Li}) - T_E - \Omega \times (I_B \Omega)$$

$$A(x) = \begin{bmatrix} \dot{r_B} \\ -C_i - G_i \\ \sum_{i=1}^{N} C_i - M_B\left(2\Omega \times \dot{r_B} + \Omega \times (\Omega \times r_B)\right) \\ -K_i \\ -N \\ wi \times e_i \\ (V_{si} - w_i \times e_i r_i)e_i \\ \dot{q_B} \\ \dot{q_{si}} \end{bmatrix}, B = \begin{bmatrix} 0 \\ 0 \\ I \\ 0 \\ I \\ 0 \\ 0 \\ 0 \\ 0 \end{bmatrix}^T, u = \begin{bmatrix} 0 \\ 0 \\ \mathrm{F}_E \\ 0 \\ T_E \\ 0 \\ 0 \\ 0 \\ 0 \end{bmatrix}$$

$$C(x) = \begin{bmatrix} I & 0 & 0 & 0\,0\,0\,0\,0 \\ 0 & A_i + D_i & B_i + E_i & F_i\,0\,0\,0\,0 \\ 0 & M_B I - \Sigma A_i & -(\Sigma B_i + M_B[r_b]^{\times}) & 0\,0\,0\,0\,0 \\ 0 & H_i & I_i & 0\,J_i\,0\,0\,0 \\ 0 & L & M & 0\,0\,0\,0\,0 \\ 0 & 0 & 0 & 0\,0\,I\,0\,0 \\ 0 & 0 & 0 & 0\,0\,0\,1\,0 \\ 0 & 0 & 0 & 0\,0\,0\,0\,I \end{bmatrix}$$

6. References

1) Robert B. Friend, "Orbital Express program summary and mission overview", Proceedings Volume 6968, Sensors and Systems for Space Applications II, 695803, 2008, https://doi.org/10.1117/12.783792
2) Wie-Jie Li, Da-Yi Cheng. et.al, "On-orbit service (OOS) of spacecraft: A review of engineering developments", Progress in Aerospace Science, Vol 108, p32-120, 2019, https://doi.org/10.1016/j.paerosci.2019.01.004
3) James Bultitude, Zach Burkhardt. et.al, "Development and Launch of the World's First Orbital Propellant Tanker", 35th Annual Small Satellite Conference, 2021
4) Takuto Ishimatsu, Oliver L. deWack, and Jeffrey A. Hoffman, et al. "Generalized Multicommodity Network Flow Model for the Earth-Moon-Mars Logistics System", Journal of Spacecraft and Rockets Vol. 53, No.1, Jan-Feb, 2016, https://doi.org/10.2514/1.A33235
5) Thomas M. Perrin, "Architecture Study for a Fuel Depot Supplied from Lunar Assets", American Institute of Aeronautics and Astronautics. https://doi.org/10.2514/6.2016-5306
6) Alessia Simonini, Michael Dreyer, et al."Cryogenic propellant management in space: open challenges and perspectives", npj microgravity 10, 2024, https://doi.org/10.1038/s41526-024-00377-5
7) Franklin T.Dodge, "THE NEW "DYNAMIC BEHAVIOR OF LIQUIDS IN MOVING CONTAINERS"", Southwest Research Institute
8) J.P.B. Vreeburg, "DYNAMICS AND CONTROL OF A SPACECRAFT WITH A MOVING PULSATING BALL IN A SPHERICAL CAVITY", Acta Astronautica Vol 40, No.2-8. 257-274, 1997, https://doi.org/10.1016/S0094-5765(97)00095-7
9) J.P.B. Vreeburg, "Measured states of Sloshsat FLEVO", National Lucht-en Ruimtevaartlaboratotium, NLR-TP-2005-518, 2005, https://doi.org/10.2514/6.IAC-05-C1.2.09

10) Mingle Deng, Baozeng Yue, “Attitude Dynamics and Control of Spacecraft with Multiple Liquid Propellant Tanks”, American Society of Civil Engineers, 2016, https://doi.org/10.1061/(ASCE)AS.1943-5525.000063
11) Lu Yu, Yue Baozeng, and Ma Bole, “Improved Moving Pulsating Ball Equivalent Model for Large-Amplitude Liquid Slosh”, AIAA Journal, Vol.60, No.8, Aug, 2022, https://doi.org/10.2514/1.J061622
12) OrbitFab, https://www.orbitfab.com/wp-content/uploads/DOC-00012-A_RAFTI_User_Guide.pdf, 2025/8/13
13) E.Todorov and W.Li, “Iterative Linear Quadratic Regulator Design for Nonlinear Biological Movement Systems”, in Proc. Int. Conf. Informat.Control, Autom. Robot., 2004, pp. 222–229.
14) E. Todorov and Yuval Tassa, “Synthesis and Stabilization of Complex Behaviors through Online Trajectory Optimization”, IEEE/RSJ International Conference on Intelligent Robots and Systems, 2012, 10.1109/IROS.2012.6386025